

Article

Interactions between DMPC Model Membranes, the Drug Naproxen, and the Saponin β -Aescin

Pia Hägerbäumer ¹, Friederike Gräbitz-Bräuer ¹, Marco Annegarn ¹, Carina Dargel ^{1,2}, Tim Julian Stank ¹, Thomas Bizien ³ and Thomas Hellweg ^{1,*}

¹ Physical and Biophysical Chemistry, Bielefeld University, Universitätsstr. 25, 33615 Bielefeld, Germany

² Institute of Physical Chemistry, University of Münster, Corrensstr. 28/30, 48149 Münster, Germany

³ Synchrotron SOLEIL, L'Orme des Merisiers, CEDEX, 91190 Saint-Aubin, France

* Correspondence: thomas.hellweg@uni-bielefeld.de; Tel.: +49-0521-106-2055

Abstract: In this study, the interplay among the phospholipid 1,2-dimyristoyl-*sn*-glycero-3-phosphocholine (DMPC) as a model membrane, the nonsteroidal anti-inflammatory drug naproxen, and the saponin β -aescin are investigated. The naproxen amount was fixed to 10 mol%, and the saponin amount varies from 0.0 to 1.0 mol%. Both substances are common ingredients in pharmaceuticals; therefore, it is important to obtain deeper knowledge of their impact on lipid membranes. The size and properties of the DMPC model membrane upon naproxen and aescin addition were characterized with differential scanning calorimetry (DSC), small- and wide-angle X-ray scattering (SAXS, WAXS), and photon correlation spectroscopy (PCS) in a temperature-dependent study. The interaction of all substances was dependent on the lipid phase state, which itself depends on the lipid's main phase transition temperature T_m . The incorporation of naproxen and aescin distorted the lipid membrane structure and lowers T_m . Below T_m , the DMPC–naproxen–aescin mixtures showed a vesicle structure, and the insertion of naproxen and aescin influenced neither the lipid chain–chain correlation distance nor the membrane thickness. Above T_m , the insertion of both molecules instead induced the formation of correlated bilayers and a decrease in the chain–chain correlation distance. The presented data clearly confirm the interaction of naproxen and aescin with DMPC model membranes. Moreover, the incorporation of both additives into the model membranes is evidenced.

Keywords: DMPC; small unilamellar vesicles (SUVs); nonsteroidal anti-inflammatory drug; naproxen; saponin; β -aescin; SAXS; WAXS; DSC; PCS



Citation: Hägerbäumer, P.; Gräbitz-Bräuer, F.; Annegarn, M.; Dargel, C.; Stank, T.J.; Bizien, T.; Hellweg, T. Interactions between DMPC Model Membranes, the Drug Naproxen, and the Saponin β -Aescin. *Pharmaceutics* **2023**, *15*, 379. <https://doi.org/10.3390/pharmaceutics15020379>

Academic Editors: Ionela Andreea Neacsu and Bogdan Stefan Vasile

Received: 18 November 2022

Revised: 13 January 2023

Accepted: 15 January 2023

Published: 22 January 2023



Copyright: © 2023 by the authors. Licensee MDPI, Basel, Switzerland. This article is an open access article distributed under the terms and conditions of the Creative Commons Attribution (CC BY) license (<https://creativecommons.org/licenses/by/4.0/>).

1. Introduction

One of the main components of biomembranes are phospholipids, which are amphiphilic molecules that consist of a substituted phosphate group as the hydrophilic head, and two hydrocarbon chains as the hydrophobic tail [1–3]. Because of their structure, phospholipids can be used for the production of biological model membranes. These are particularly useful in studying the interaction of biomolecules and drugs with the lipids forming the membrane [4,5]. In aqueous solution, phospholipids tend to assemble into spherical compartments, so-called vesicles that comprise one or more lipid bilayers [6]. Via extrusion through a porous membrane or sonication, small unilamellar vesicles (SUVs) are obtained [7,8]. SUVs can, for instance, be used for medical applications such as drug delivery [9–11].

Phospholipid membranes show interesting temperature-dependent phase behavior [12]. An often-studied phospholipid is the synthetically produced 1,2-dimyristoyl-*sn*-glycero-3-phosphocholine (DMPC), which possesses a phosphatidylcholine unit as the hydrophilic and two tetradecane fatty acid esters as the hydrophobic part [3]. Its molecular structure is shown in Figure 1a. At low temperatures, the DMPC membrane is present in a gel-like L_{β} phase in which the lipid molecules are ordered in an *all-trans* configuration. At 13.7 °C, the

lipid molecules rearrange in a prephase transition into the $P_{\beta'}$ phase, where the molecules are ordered hexagonally. The main phase transition temperature T_m of DMPC is reached at 24 °C; above this temperature, the membrane adopts a liquid crystalline phase L_{α} where the molecules are arranged in *gauche* configuration [13].

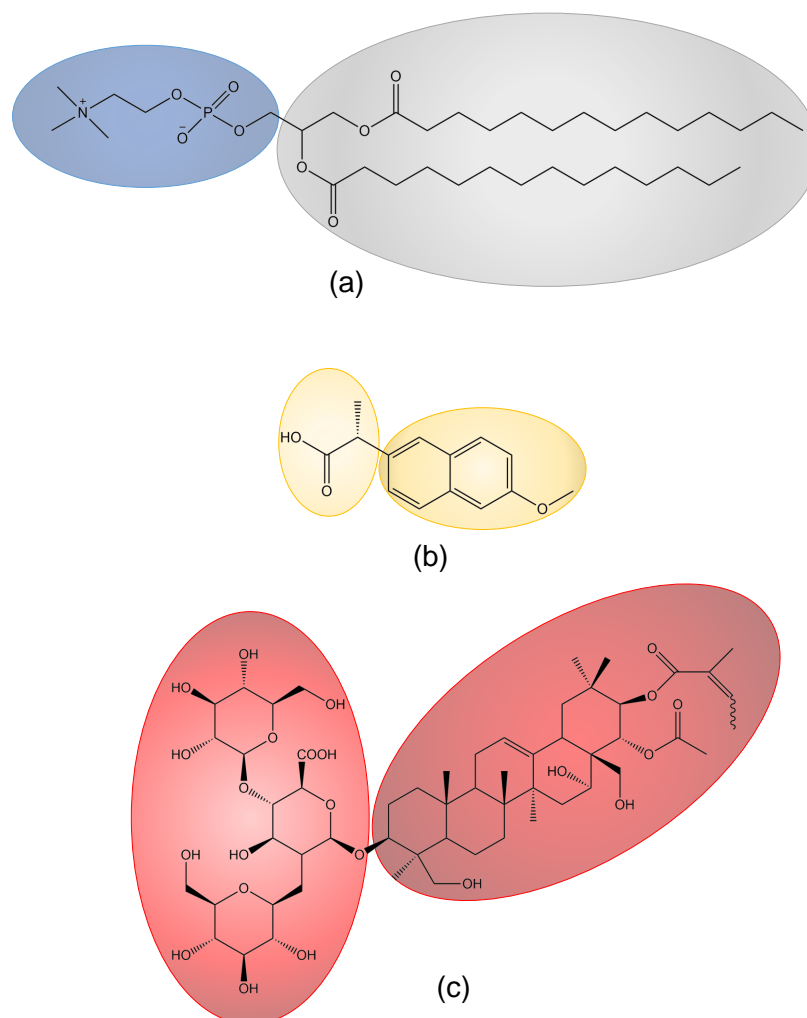


Figure 1. Chemical structures of (a) phospholipid DMPC, (b) NSAID naproxen, and (c) saponin β -aescin.

Interaction with other substances or even their intercalation into the membrane can significantly modify the membrane's properties. Nonsteroidal anti-inflammatory drugs (NSAIDs) are therapeutic drugs that inhibit the cyclooxygenase pathway; hence, they are used against fever, inflammation, and pain [14–16]. Common representatives are naproxen, ibuprofen, and diclofenac [17], which all interact with phospholipid membranes [15,16,18–21]. In this study, naproxen (Figure 1b) is used as representative of this substance class and in comparison to the prior investigated ibuprofen [10,22,23].

A study by Lichtenberger et al. states that NSAIDs bind to zwitterionic phospholipids via both hydrophobic and electrostatic interactions. The latter are established by the positively charged nitrogen of the phospholipid (see Figure 1a) and the carboxyl group of the NSAID, which is normally negatively charged [24]. Due to these interactions and the related perturbation of the regular lipid membrane through the integration of the NSAID, the T_m of these membranes is lowered [15,22]. Moreover, membrane fluidity can be affected by the integration of the NSAID into the lipid membrane [20].

Saponins are natural biosurfactants and can be isolated from plants [25]. Their name originates from the Latin word “sapo”, meaning “soap”, and is related to their foaming

properties and their use as washing agents. They can be classified by their molecular backbone into triterpenes and steroids. The head group consists of one or more sugar moieties [26–29]. Saponins also interact with phospholipid membranes, red blood cells, and cancer cells, as they are able to alter the membrane properties and structure [30–35]. The well-known saponin β -aescin is studied here [36,37]. Aescin is an extract from the seeds of the horse chestnut (*Aesculus hippocastanum*) [38] and is a mixture of different saponins with a triterpenic backbone linked via glucuronic acid to two glucose units as the head group (Figure 1c) [39,40]. Aescin on its own forms micelles in aqueous solutions. The critical micelle concentration (*cmc*) of aescin is 0.33 mM [39]. It has an anti-inflammatory effect, and is used against edema and venous insufficiency [41,42].

The interaction of aescin with DMPC model membranes was intensively studied in dependence on the concentration of the saponin aescin, and a concentration-dependent phase behavior was observed [43]. At low aescin concentrations, the insertion of aescin into the lipid membrane was evidenced, which was accompanied by the lowering of T_m and an increase in vesicle size [44]. Increasing the aescin concentration up to its *cmc* leads to the formation of correlated membrane structures, either intact and aggregated vesicles or larger correlated membrane fragments [31]. At concentrations above the *cmc* of aescin, the lipid membrane is lastly completely solubilized into bicelles [45]. The whole phase behavior in dependence on aescin concentration and temperature was summarized in a recent review article [43]. In addition to the phase behavior of the DMPC–aescin mixture, the interaction of DMPC with the NSAID ibuprofen and the saponin aescin was also investigated [22]. As has been shown in this work, ibuprofen and aescin interact with the model membrane and change its properties on a molecular level. A lowering of T_m was observed.

In comparison to the DMPC–ibuprofen–aescin system, here, the interaction of naproxen and aescin with DMPC model membranes is investigated. Although both mentioned substances are painkillers and cyclo-oxygenase inhibitors, naproxen is used especially for menstrual pain. In their pharmacological properties, they particularly differ in their elimination half-life and thereby their exposure to human cells. Where ibuprofen only has a half-life in the serum of 1.8 h to 2 h, naproxen is significantly more persistent, with a half-life of 16 h to 36 h [46,47]. These disparities can be attributed to their different molecular structures. While both 2-arylpropionates contain a stereocenter in the α -position of the propionate group, their molecular backbone differs significantly. Ibuprofen, on the one hand, is based on an alkylated benzene ring. Naproxen, on the other hand, has a larger naphthalene unit with a more polar methoxy group as its molecular backbone. Hence, both NSAIDs differ in size, planarity, and polarity. These important differences render it interesting to study the influence of naproxen on lipid membranes in the presence of aescin, as a different interaction with membranes might be the case. In the human body, naproxen is usually ingested through the intake of medication; for example against menstrual pain, aescin could be contained in certain foods and vein medications. Due to the fact that naproxen is a common analgesic, and aescin is used in vein tablets, it is important to consider the interaction and analyze the influence of the two substances on lipid membranes on a molecular scale [19].

This study was conducted at a physiological pH value of 7.4 in a temperature-dependent manner. We applied the methods of differential scanning calorimetry (DSC), small- and wide-angle X-ray scattering (SAXS, WAXS), and photon correlation spectroscopy (PCS), since their combination is ideally suited for the investigation of various soft-matter and nanoscopic systems [48–50]. The influence of naproxen and aescin addition on the DMPC membrane's T_m and the lipid membrane size parameters, derivable from different scattering techniques, is examined.

2. Materials and Methods

2.1. Chemicals

For vesicle preparation, the phospholipid 1,2-dimyristoyl-*sn*-glycero-3-phosphocholine (DMPC, >99%, CAS: 18194-24-6, Lipoid GmbH, Ludwigshafen, Germany), the NSAID

naproxen (CAS: 22204-53-1, Sigma-Aldrich, Munich, Germany) and the saponin β -aescin ($\geq 95\%$, CAS: 6805-41-0, Sigma-Aldrich) were used without further purification. Chloroform ($\geq 99.8\%$, CAS: 67-66-3) was purchased from Fisher Chemicals, Waltham, MA, USA. Purified water (arium pro VF System, Sartorius AG, Germany) was used for the aqueous sodium phosphate buffer (50 mM, pH 7.4).

2.2. Vesicle Preparation

DMPC (15 mg mL⁻¹) and naproxen (10 mol%) were dissolved in chloroform in a round-bottom flask. The molar fraction of naproxen or aescin $w(\text{naproxen/aescin})$ was defined according to Equation (1).

$$w(\text{naproxen/aescin}) = \frac{n_{\text{naproxen/aescin}}}{n_{\text{DMPC}} + n_{\text{naproxen}} + n_{\text{aescin}}} \quad (1)$$

After removing the solvent using a rotary evaporator at room temperature in vacuo, the samples were stored overnight in a drying oven (60 °C), lastly yielding a thin DMPC–naproxen film, which was rehydrated with different aescin amounts between 0.0 mol% to 1.0 mol% in a phosphate buffer. The vesicles were enlarged with five freeze–thaw–cycles in liquid nitrogen (−196 °C) and a water bath (40 °C), and then stored frozen at −20 °C. The vesicles were extruded at least 15 times at T above T_m with an extruder (Avanti Polar Lipids Inc., Alabaster, AL, USA, membrane pore size: 50 nm, Whatman) right before performing any measurement.

2.3. Differential Scanning Calorimetry (DSC)

DSC experiments were performed by employing a differential scanning heat-flow calorimeter (DSC Q100, TA Instruments, New Castle, DE, USA) to investigate the phase behavior of the lipids in the bilayer. The samples were measured in a hermetically sealed aluminum pan that had been heated up to 40 °C and cooled down to 7 °C with heating and cooling rates of 7 °C/min as a pre-equilibration. Afterwards, the sample was heated up to 40 °C with a heating rate of 0.5 °C/min. The measured heat flow ΔP was the difference between the heat flow of the sample P_S and the reference P_0 (pan filled with air). The peak maxima of the thermograms, which give T_m , were determined with Lorentzian fits.

2.4. Small- and Wide-Angle X-ray Scattering (SAXS and WAXS)

SAXS and WAXS measurements were performed on the SWING beamline at synchrotron SOLEIL, France. The extruded vesicles were measured with a Linkam-Stage (HFSX350, Linkam Scientific, Salfords, UK) in a flowthrough Kapton[®] capillary (1 mm, GoodFellow GmbH, Hamburg, Germany) in a temperature range of 10–45 °C in increments of 5 °C. Samples were measured at sample-to-detector distances of 0.5 and 6 m to cover a q -range of 0.004 Å⁻¹ to 1.8 Å⁻¹. The magnitude of the scattering vector q depends on wavelength λ , refractive index n ($n = 1$ for X-rays), and scattering angle θ (Equation (2)).

$$q = \frac{4\pi n}{\lambda} \cdot \sin\left(\frac{\theta}{2}\right) \quad (2)$$

The wavelength was 1.033 Å, and the exposure time was 20 × 1 s. Scattering patterns were detected by an EigerX 4M (Dectris, Baden, Switzerland). The data were evaluated with Foxtrot software (version 3.3.4) [51]. The scattering curves were normalized with respect to intensity, transmission, sample thickness, and exposure time, with the background subtracted and averaged.

By analyzing the position of the peak maximum q_{peak} of the WAXS curves, information about the changes of the membrane structure regarding the chain–chain correlation distance d_{WAXS} could be obtained [52]. The peak maximum was precisely determined

with a Lorentzian fit and converted into the chain–chain correlation distance applying the following equation (Equation (3)).

$$d_{\text{WAXS}} = \frac{2\pi}{q_{\text{peak}}} \quad (3)$$

The SAXS data were treated with the dynamic rebin formalism in SAXSutilities to improve statistics of individual data points at high q values (minimal steps: 1, minimal delta: 0.005) [53]. The SAXS curves were analyzed by using the PCG software package by O. Glatter [54,55]. An indirect Fourier transformation (IFT) was performed with the GIFT program to determine the pair distance distribution function $p(r)$ and the radius of gyration R_G . The vesicle was divided into the membrane part at low r -values and the overall structure at high r -values up to r_{max} . At low r -values up to 75 Å, 10 cubic B-splines with 10 points per spline were used to approximate the bilayer regime. To describe the vesicular morphology, 15 cubic splines from 75 Å to r_{max} with 10 points per spline were used. R_G was calculated from the integral of the determined $p(r)$ function by Equation (4).

$$R_G^2 = \frac{\int_0^{\infty} p(r)r^2 dr}{2 \int_0^{\infty} p(r) dr} \quad (4)$$

Lastly, the modified Kratky–Porod (MKP) analysis was performed to determine the membrane thickness $d_{\text{m,MKP}}$ at $T = 10$ °C [30,56]. For that, $I \cdot q^4$ was plotted vs. q and fitted with a polynomial of fourth order. Then, the maximum was determined, and $d_{\text{m,MKP}}$ was calculated via the relation in Equation (5).

$$d_{\text{m,MKP}} = \frac{2\pi}{q_{\text{max}}} \quad (5)$$

2.5. Photon Correlation Spectroscopy (PCS)

The hydrodynamic radius R_H of the vesicles was determined via angle-dependent PCS measurements at $T = 10$ °C. Samples were measured in NMR tubes with a 3D LS Spectrometer Pro (LS instruments, Fribourg, Switzerland) equipped with a HeNe Laser (632.8 nm, 1145P; JDSU, Milpitas, CA, USA), decaline index-matching vat, automated goniometer and two detectors (SPCM-AQRH-13-FC, Perkin Elmer, Waltham, MA, USA). The measurements were performed in 3D cross-mode to remove multiple scattering in a scattering angle range of 40° to 110° with increments of 5° with a measuring time of five times 200 s per angle. The autocorrelation function was generated with a multiple- τ digital correlator and later analyzed by means of inverse Laplacian transformation (CONTIN) to obtain the mean relaxation rate Γ [57,58]. R_H was calculated via the Stokes–Einstein equation (Equation (6)) with Boltzmann constant k_B , temperature T , viscosity of the solvent η , and translational diffusion coefficient D_T . The latter was derived from the slope of the linear dependency of Γ and the squared magnitude of the scattering vector q^2 (Equation (7)) [59].

$$R_H = \frac{k_B \cdot T}{6 \cdot \pi \cdot \eta \cdot D_T} \quad (6)$$

$$\Gamma = D_T \cdot q^2 \quad (7)$$

The viscosity of water was calculated in dependence of the temperature [60].

3. Results and Discussion

The phospholipid 1,2-dimyristoyl-*sn*-glycero-3-phosphocholine (DMPC) with a constant amount of the nonsteroidal anti-inflammatory drug naproxen of 10 mol% and low amounts of the saponin β -aescin (0.0 mol% to 1.0 mol%) were investigated. In all cases, the aescin concentration was lower than the *cmc* of aescin [39]. After extrusion, the formation

of small and stable particles was revealed through the slight blue opalescence of the samples at temperatures below the main phase transition temperature T_m . Most likely, these structures were small unilamellar vesicle SUVs. At temperatures above T_m , the samples turned turbid, and a white precipitate formed that indicated that the vesicles could have begun to aggregate and form larger units. The influence of both additives on the lipid phase behavior, and on the vesicle and membrane structure is analyzed and discussed in the following subsections.

3.1. Differential Scanning Calorimetry (DSC): Determination of T_m

The DMPC SUVs were investigated via differential scanning calorimetry (DSC) in order to resolve the phase transition and determine the T_m of the lipid bilayer, at which the temperature-induced conformational change of the hydrocarbon chains from *all-trans* into *gauche* takes place. The endothermic DSC thermograms are shown in Figure 2a. The maximum of the sharp peak gave T_m of the bare DMPC SUVs ($(24.64 \pm 0.06)^\circ\text{C}$). This value is in good agreement with T_m determined by Sreij et al. [22]. The addition of naproxen led to a significant decrease in the T_m of the lipid membrane, as seen from the comparison of the black and red curves in the DSC-thermograms (Figure 2a). The shift in T_m due to naproxen incorporation was also visible in data from Manrique-Moreno et al. and resulted from the interaction of the phospholipid headgroup with the hydrophilic part of the drug [15,61]. The increasing amount of aescin led to a further reduction in T_m , down to $(24.00 \pm 0.06)^\circ\text{C}$ for an aescin amount of 1 mol%. Above an aescin amount of 0.6 mol%, a shoulder was noticeable that emerged to a broad second peak at temperatures below T_m . The presence of this additional signal was attributed to the formation of aescin-rich and aescin-poor domains [43]. The T_m of the lipid membrane and of the aescin-rich domains was plotted as a function of $w(\text{aescin})$ in Figure 2b. The incorporation of additives naproxen and aescin interrupted the ordered structure of the lipid molecules and led to a perturbation in the membrane. Therefore, less energy had to be supplied to complete the phase transition, and T_m decreased. The effects described here are already found in the DMPC–ibuprofen–aescin system [22]. Naproxen might not influence the formation of these aescin domains with different phase transition temperatures.

3.2. Wide-Angle X-ray Scattering (WAXS): Determination of d_{WAXS}

The vesicles containing DMPC, naproxen, and aescin were analyzed with wide-angle X-ray scattering (WAXS). The temperature-dependent scattering curves of DMPC with 10 mol% naproxen and 0.0 mol% and 0.8 mol% aescin are exemplarily shown in Figure 3. The WAXS measurements were performed at a temperature range of 10–45 °C in increments of 5 °C. The WAXS curves of samples with other $w(\text{aescin})$ looked similar and all are presented in the Supplementary Information (Figures S1 and S2). The open circles at around 1.3 \AA^{-1} mark artifacts that occurred in both the sample and the background measurement, and were not considered in the analysis. Due to thermally induced aggregation, scattering curves for DMPC with naproxen and 1 mol% aescin are only shown up to 25 °C (Figure S2). The WAXS signals below T_m showed a typical narrow shape, whereas the signal broadened in the L_α phase above T_m [62].

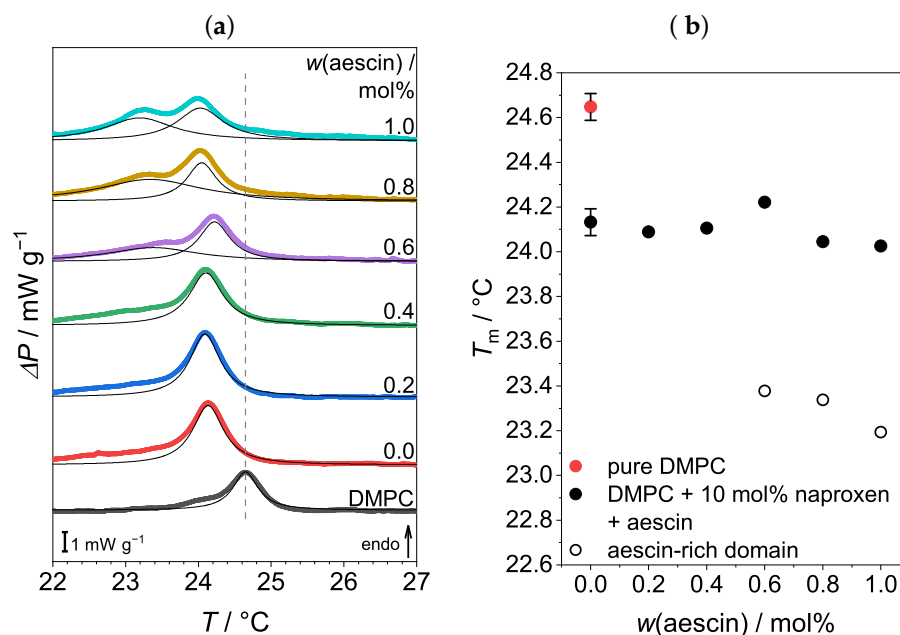


Figure 2. (a) Endothermic DSC thermograms of vesicles containing DMPC, 10 mol% naproxen, and different amounts of aescin. The black lines show the Lorentzian fits to determine the maxima of the measured signals. The dashed gray line indicates the T_m of pure DMPC vesicles at (24.64 ± 0.06) °C. The addition of naproxen induced a shift of T_m to lower temperatures. Aescin amounts from 0.6 mol% and higher led to the appearance of a second peak below T_m . (b) The plot of T_m of the DMPC lipid membrane and the aescin-rich domains against $w(\text{aescin})$. As an example, the error bars for two data points are given. For the sake of clarity, the other data points were plotted without error bars.

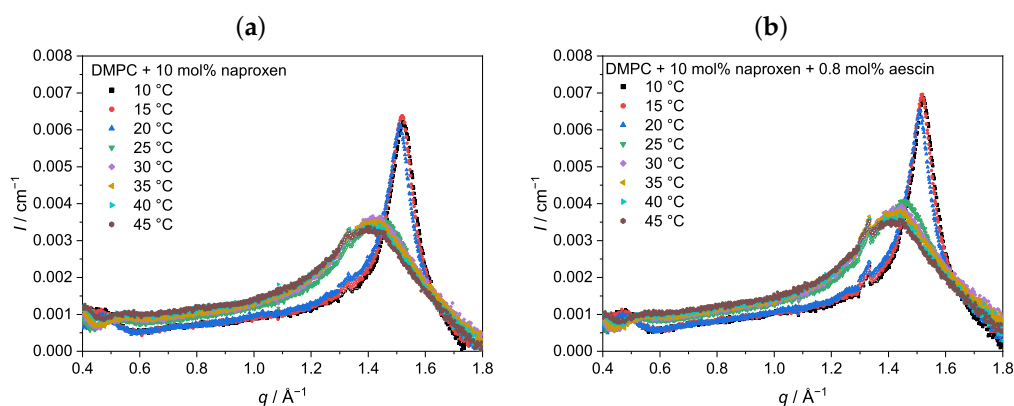


Figure 3. WAXS curves of DMPC vesicles with (a) 10 mol% naproxen and (b) 10 mol% naproxen and 0.8 mol% aescin at different temperatures. The maximum of the WAXS signal shifted to lower q -values with increasing temperature. The open circles around 1.3 \AA^{-1} mark artifacts that were not considered for evaluation.

The peak maximum q_{peak} shifted with increasing temperature to lower q -values and changed from a sharp, narrow peak below T_m into a broadened peak above T_m . Additionally, the most significant change in q_{peak} was visible around T_m . The same trend had been observed by Sreij et al. in small unilamellar DMPC vesicles with ibuprofen and aescin [22]. d_{WAXS} was determined by Equation (3) from q_{peak} and is plotted in Figure 4. Due to the conformational change of the lipids in the bilayer during the main phase transition, d_{WAXS} is a temperature-dependent parameter. At temperatures below T_m , d_{WAXS} was the smallest, as the lipid DMPC was in the $L_{\beta'}$ phase where the chains were packed in a hexagonal lattice [13]. An increase in temperature up to T_m resulted in a slight increase in d_{WAXS} due

to thermal expansion. A comparison of the samples with and without naproxen and aescin shows that the incorporation of both did not impact d_{WAXS} as long as $T < T_m$.

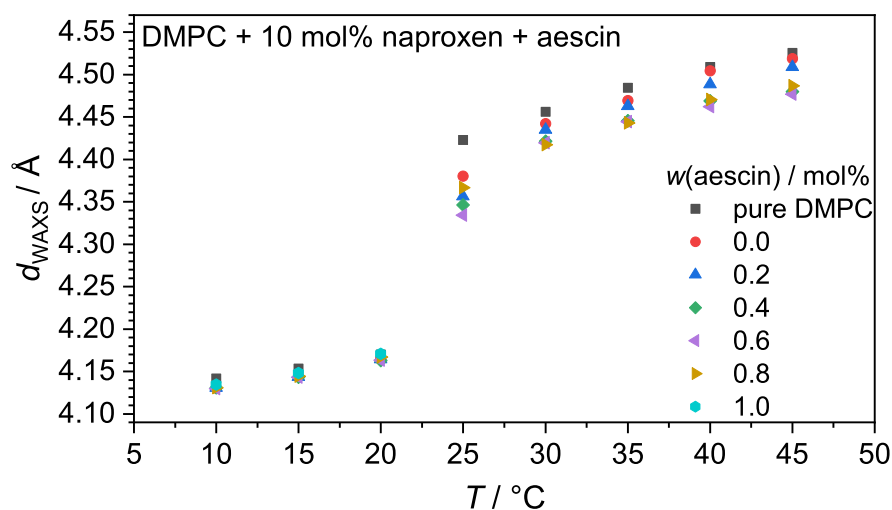


Figure 4. Temperature-dependent d_{WAXS} values of the DMPC vesicles with naproxen and aescin, calculated from the peak maximum q_{peak} via Equation (3).

Upon an increase of T above T_m , the lipid underwent the main phase transition into the L_α phase, in which d_{WAXS} is increased due to the more flexible rearrangement of the lipid molecules. Compared to pure DMPC vesicles, d_{WAXS} slightly decreased if 10 mol% naproxen was added to the DMPC sample. A further decrease upon aescin addition and with increasing $w(\text{aescin})$ was observed, additionally. The accumulation of aescin into the DMPC membrane, which could be deduced from DSC, led to a compression of the DMPC molecules, which was expressed in a smaller d_{WAXS} value. Hence, the DMPC membrane in the L_α phase was stabilized in the presence of aescin.

3.3. Analysis by Small-Angle X-ray Scattering (SAXS)

Small-angle X-ray scattering (SAXS) measurements of the DMPC–naproxen–aescin samples were performed at the SWING beamline of the Soleil synchrotron. Datasets for DMPC vesicles containing naproxen and DMPC vesicles containing naproxen and 0.8 mol% aescin are shown exemplarily in Figure 5. SAXS data for all samples are presented in the Supplementary Information (Figure S3). Scattering data of the reference system, pure DMPC, are shown in Figure S3a. Pure DMPC vesicles were stable in the investigated temperature range. Below and above T_m , the formation of aggregated structures was not observed (Figures S3 and 9).

Below T_m , the scattering curves were, in the two cases of DMPC with 10 mol% naproxen (Figure 5a), and DMPC with 10 mol% naproxen and 0.8 mol% aescin (Figure 5b), characteristic for unilamellar vesicles [30]. The oscillations at low q -values indicate a rather narrow distribution of the vesicle size, and the signal at around 0.1 \AA^{-1} represents the form factor of the lipid membrane. When T_m was reached, the lipid membrane underwent a conformational change from the L'_β into the L_α phase (at $T \geq 25 \text{ }^\circ\text{C}$). Hence, the continuous DMPC membrane lost its dense packing, and penetration of water molecules into the lipid membrane was eased [63]. As a consequence of that, the electron density difference between the membrane and the solvent decreased, so that a size resolution of the vesicle structure was not possible anymore due to the decreased scattering intensity at low q . At the high q -region, additionally to the membrane form factor, a structure factor appeared if an additive was present in the sample. If only naproxen had been added to the DMPC, the correlation signal at 0.1 \AA^{-1} was very weak, but became more intense if the aescin content was also increased. This indicates the formation of correlated bilayer structures induced by the presence of aescin. Additionally, a second signal q_2 at around 0.2 \AA^{-1} appeared and,

like the signal q_1 at 0.1 \AA^{-1} , increased in intensity with increasing $w(\text{aescin})$. From the ratio of both signals ($2q_1 \approx q_2$) it can be concluded that a lamellar-phase-like arrangement was present in the sample.

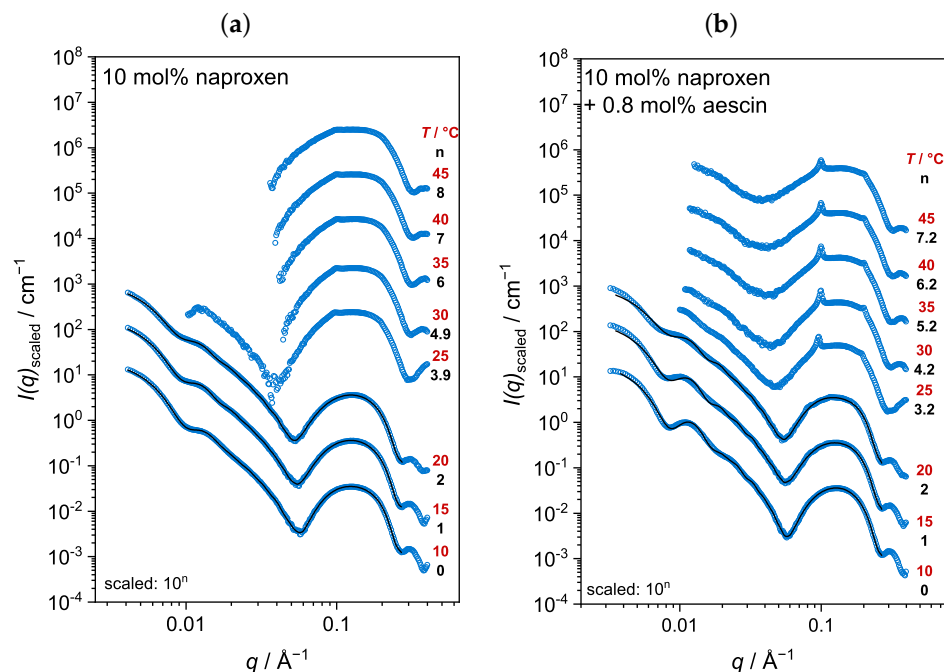


Figure 5. SAXS curves of (a) DMPC vesicles with 10 mol% naproxen and (b) vesicles with 10 mol% naproxen and 0.8 mol% aescin at different temperatures (see red numbers on the right). Scattering curves were scaled by powers of 10 for better visibility. Solid lines are IFT approximations to the scattering data.

In the following, first, the pair distance distribution function $p(r)$ and the radius of gyration R_G are determined with indirect Fourier transformation (IFT) for all samples at $T < T_m$. Afterwards, the membrane thickness $d_{m,MKP}$ is calculated by the modified Kratky–Porod (MKP) method for all samples at $T = 10 \text{ }^\circ\text{C}$. Lastly, we focus on the membrane aggregation at $T > T_m$.

3.3.1. Pair Distance Distribution Function $p(r)$ and Radius of Gyration R_G by Indirect Fourier Transformation (IFT) at $T < T_m$

The indirect Fourier transformation (IFT) method is a model-independent tool to determine the pair distance distribution function (PDDF or $p(r)$) and thereby the radius of gyration R_G of a scattering particle [54,55]. Only samples recorded at $T < T_m$ were considered for evaluation because, for these samples, the overall size and structure were accessible from the low q -range. The normalized $p(r)$ functions at temperatures of $10 \text{ }^\circ\text{C}$, $15 \text{ }^\circ\text{C}$ and $20 \text{ }^\circ\text{C}$ are shown in Figure 6a–c. Oscillation at low distances r is a typical characteristic of a lipid membrane with head-tail contrast that occurs due to the difference in the electron densities of the lipids head and tail parts within the lipid bilayer [64]. The maximum of the $p(r)$ functions shifted to higher distances with increasing $w(\text{aescin})$. This indicates that the vesicles grew.

R_G , obtained by the $p(r)$ function from Equation (4), was plotted as a function of $w(\text{aescin})$ at $10 \text{ }^\circ\text{C}$, $15 \text{ }^\circ\text{C}$ and $20 \text{ }^\circ\text{C}$ in Figure 6d. The addition of naproxen to the DMPC vesicles showed no significant impact on R_G at a constant temperature. DSC clearly showed the incorporation of naproxen into the lipid membrane, but this incorporation seems not to influence the R_G of the vesicle. However, R_G increased with the addition of aescin and increasing $w(\text{aescin})$, which indicates successful incorporation of naproxen and aescin into the lipid membrane. At constant $w(\text{aescin})$ but increasing temperature, an enlargement of

the vesicle size was observed due to the prephase change from L_{β} into P_{β}' , which had also been seen by Sreij et al. [31].

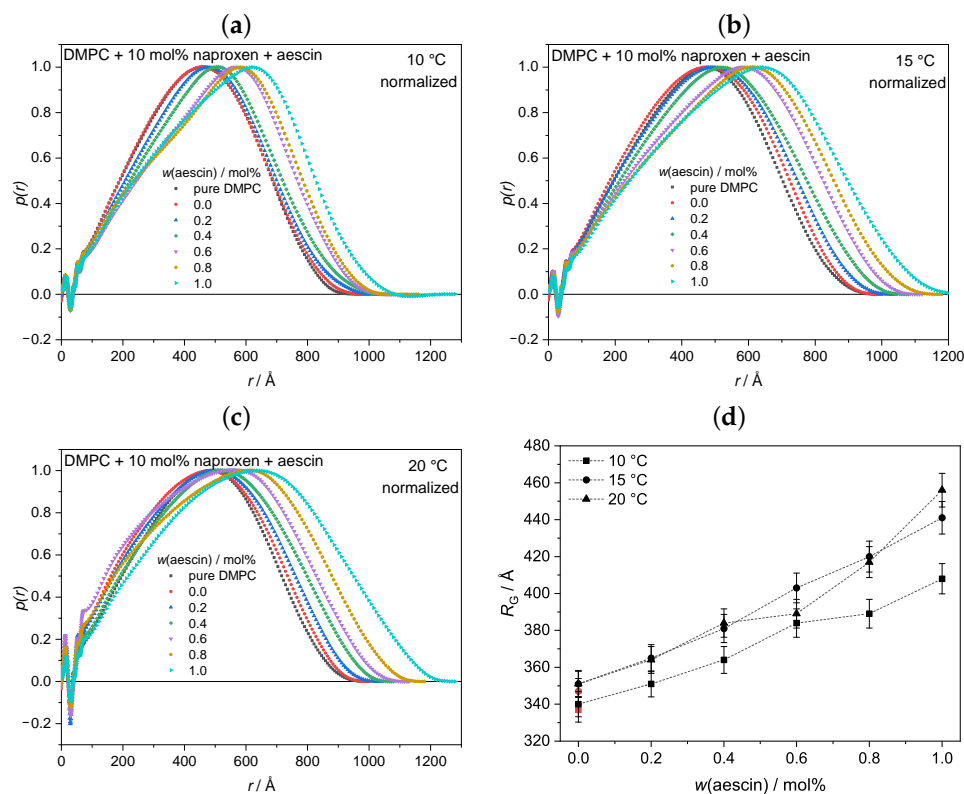


Figure 6. Pair distance distribution functions $p(r)$ of pure DMPC vesicles and vesicles containing naproxen and aescin at (a) 10 °C, (b) 15 °C and (c) 20 °C. Functions were normalized to the maximum of $p(r)$ for better comparability. (d) Radius of gyration R_G of DMPC vesicles containing naproxen and different amounts of aescin against $w(\text{aescin})$ at $T = 10$ °C, 15 °C and 20 °C. The dashed lines are only visual guides. The red symbols depict R_G of pure DMPC vesicles.

3.3.2. Membrane Thickness $d_{m,\text{MKP}}$ by Modified Kratky Porod (MKP) at $T < T_m$

The membrane thickness $d_{m,\text{MKP}}$ of nonaggregating vesicles can be analyzed with the model-independent modified Kratky–Porod (MKP) method [18,30]. Aggregation effects could be excluded for samples up to 0.4 mol% aescin for $T < T_m$, but samples from 0.6 mol% aescin showed an indication of aggregation at $T = 15$ °C. Therefore, only data recorded at 10 °C were considered for evaluation here. On the basis of SAXS data, $I(q) \cdot q^4$ was plotted against q . Examples for DMPC vesicles containing naproxen, and vesicles with naproxen and 0.8 mol% aescin are shown in Figure 7. The resulting plots were fitted with a fourth-order polynomial to obtain the maximal q -value q_{max} that was used to calculate $d_{m,\text{MKP}}$ according to Equation (5). The calculated $d_{m,\text{MKP}}$ values were plotted as a function of $w(\text{aescin})$ at $T = 10$ °C (Figure 8).

The bilayer thickness of pure DMPC vesicles at $T = 10$ °C was (34.72 ± 0.38) Å, which nicely corresponded to the value obtained by Sreij et al. [30], also determined for bare DMPC SUVs. Within the accuracy of the method, no significant change in $d_{m,\text{MKP}}$ was observed upon the addition of naproxen or upon the increase in $w(\text{aescin})$. Therefore, the incorporation of both additives had no influence on the thickness of the DMPC membrane. An explanation might be that aescin was filling gaps in the membrane that had been created by the incorporation of naproxen.

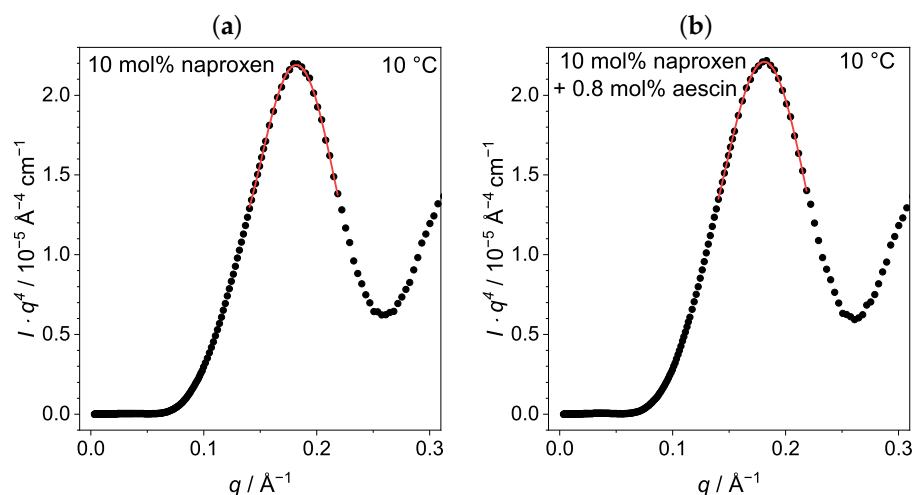


Figure 7. MKP plots for DMPC vesicles (a) with 10 mol% naproxen and (b) with 10 mol% naproxen and 0.8 mol% aescin at $T = 10$ °C. Red lines are fourth-order polynomial fits.

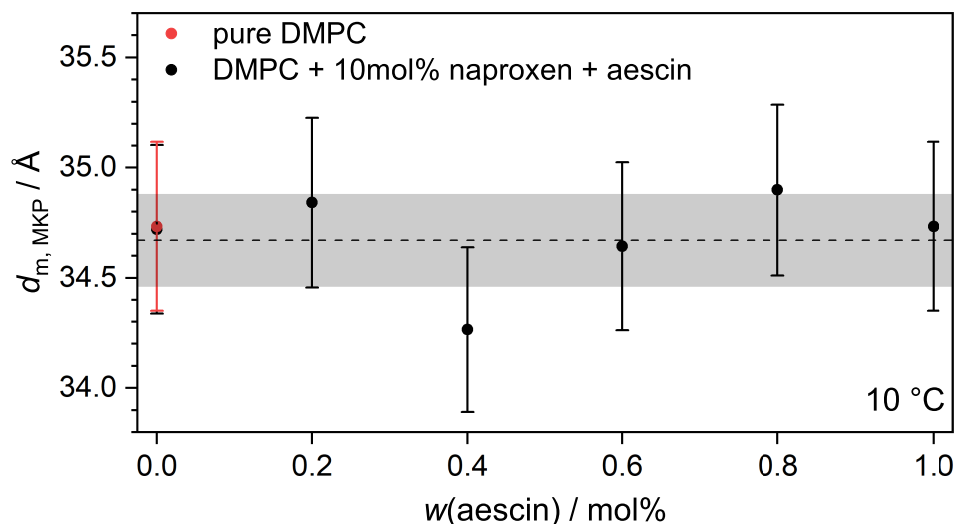


Figure 8. Membrane thicknesses $d_{m, \text{MKP}}$ of vesicles determined via MKP approximation at $T = 10$ °C in dependence of $w(\text{aescin})$. The dashed line gives the mean value of $d_{m, \text{MKP}}$ at (34.67 ± 0.21) Å. The red circle depicts the membrane thickness of pure DMPC vesicles.

3.3.3. Membrane Structure at $T > T_m$

Increasing the temperature above T_m caused the lipid membrane to undergo a structural transition from the $P_{\beta'}$ into the L_{α} phase. A higher space requirement of the single DMPC molecules accompanied this transition (compare Figure 4). The membrane itself became less dense, which caused the contrast of the overall vesicle to decrease. The size and structural determination from the low q -region was not possible anymore because no significantly differing data from the scattering background could be recorded. However, information about the membrane structure itself was still accessible. Representatively for all $T > T_m$, the scattering data at 40 °C are shown in Figure 9a for all samples investigated. For samples containing aescin at $T > T_m$, i.e., from 30 °C onwards, two additional peaks in the bilayer region at around 0.1 \AA^{-1} as first-order and at around 0.2 \AA^{-1} as a second-order signal appeared. These signals, resulting from the formation of correlated membrane structures, became more intense with increasing $w(\text{aescin})$. The ratio between the signal positions ($2q_1 \approx q_2$) indicates the formation of a lamellar structure, and the rising peak intensity indicates the formation of a higher number of correlated bilayers within this lamellar arrangement.

The repeat distance of the correlated lamellae d_{lam} could be calculated from the position q_1 of the first order correlation signal, located at around 0.1 \AA^{-1} , with the relation $d_{\text{lam}} = 2\pi/q_1$. This distance comprises an entire bilayer and an interstitial water layer. Figure 9b depicts d_{lam} as a function of $w(\text{aescin})$. For aescin-containing samples, d_{lam} remained constant, which indicates that a further addition of aescin had no influence on the correlation distance of the lamellar stack. For the system containing only DMPC and naproxen, a higher repeat distance was observed, which might have been an artifact from the weak and quite broad signal.

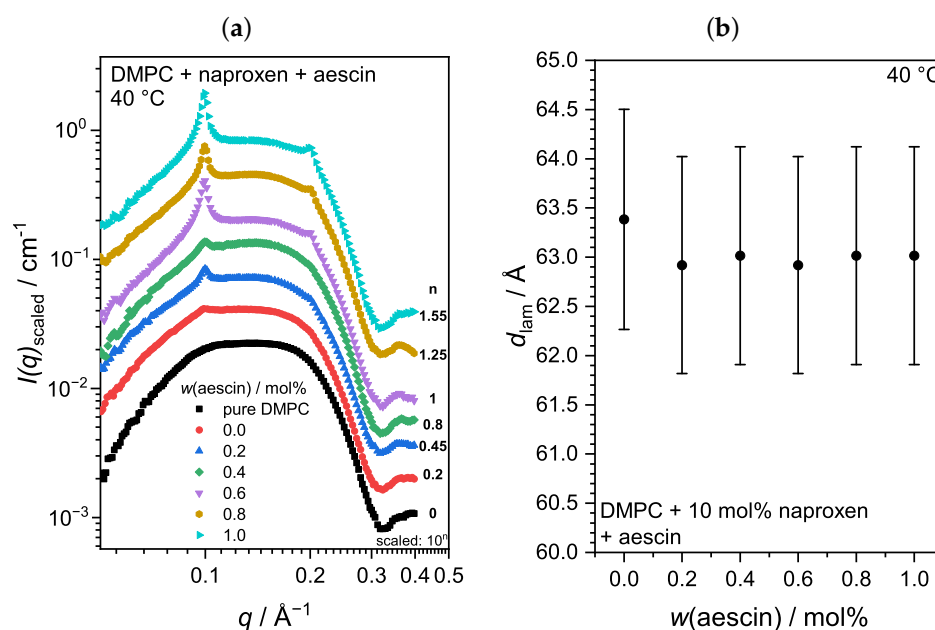


Figure 9. (a) SAXS curves of DMPC vesicles with 10 mol% naproxen and varying amounts of aescin at $T = 40 \text{ }^\circ\text{C}$. Scattering curves are scaled by powers of 10 for better visibility. (b) Lamellar repeat distance d_{lam} of the correlated bilayers calculated from the maximum of the first order Bragg peak at $T = 40 \text{ }^\circ\text{C}$.

For the samples containing 0.6 mol% or more of aescin, correlation signals in the membrane region were even visible at temperatures below T_m (see Figure S3). In contrast to $T > T_m$, three distinct peaks appeared, indicating the formation of different structures with different spacing. The SAXS curves of all samples at $T = 20 \text{ }^\circ\text{C}$ are shown in Figure S4 in the Supplementary Information. This is in analogy to the naproxen-free system, in which these kinds of signals were observed for aescin contents of 1 mol% to 5 mol% and at temperatures around T_m [31]. The correlated membrane structures can be interpreted as precursors of solubilized membrane fragments and finally completely decomposed bicelles. Therefore, the present observation gives a hint towards the increased ability of aescin to decompose a lipid vesicle membrane in presence of naproxen [31,43]. This behavior is analogous to the previously studied ibuprofen–DMPC system with added aescin [22].

3.4. Photon Correlation Spectroscopy (PCS): Determination of R_H below T_m

To avoid multiple scattering effects, the vesicles were measured in a 3D photon cross-correlation spectroscopy (3D-PCS) setup at different angles at $T = 10 \text{ }^\circ\text{C}$ to determine the hydrodynamic radius R_H below T_m . Moreover, at low T , the formation of aggregates is mostly avoided. The plots of relaxation rate Γ for DMPC vesicles with naproxen and vesicles with naproxen and 0.8 mol% aescin are shown in Figure 10. In addition, the plots for the other samples are shown in the Supplementary Information (Figures S5 and S6).

Via Equation (6), R_H can be calculated. The hydrodynamic radius was plotted as a function of $w(\text{aescin})$ in Figure 11. Pure DMPC vesicles have a R_H of $(474 \pm 24) \text{ \AA}$ at $T = 10 \text{ }^\circ\text{C}$. R_H remained constant upon addition of naproxen and increased with increasing

$w(\text{aescin})$ from around 450 Å to 1010 Å, which indicates the successful incorporation of aescin molecules into the lipid membrane. This trend was also shown by Sreij et al. [44]. R_H was larger than R_G because the hydrodynamic radius includes a hydration shell that is enlarged compared to normal lipids due to the presence of the sugar moieties. A comparison of the two radii is shown in Figure S7. The values of R_H and PDI are given in Table S1. Both radii increased with increasing $w(\text{aescin})$. The high apparent R_H for the DMPC vesicles containing naproxen and 1.0 mol% aescin (open circle (Figure 11)) might have been caused by aggregation of the vesicles and was not considered.

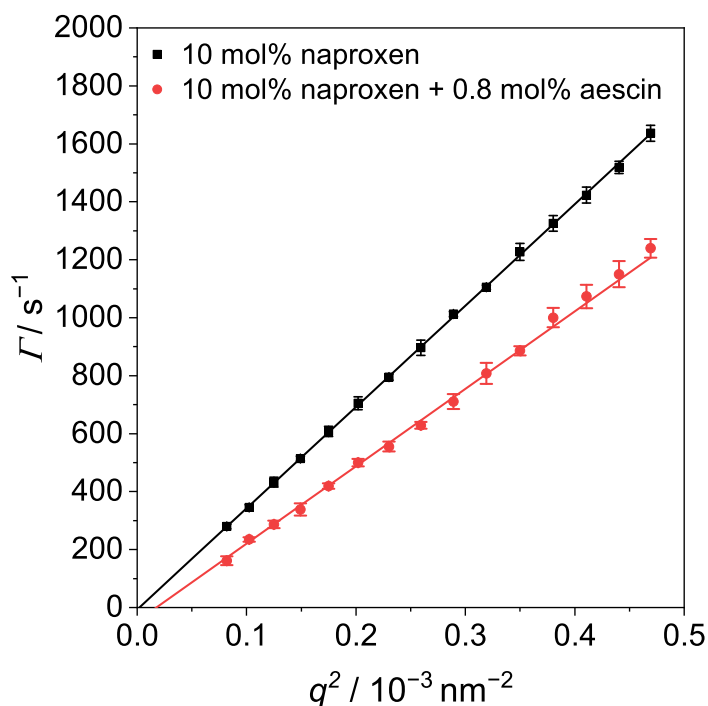


Figure 10. Γ plotted against q^2 measured by angle-dependent PCS at $T = 10^\circ \text{C}$ for DMPC vesicles with 10 mol% naproxen and vesicles with 10 mol% naproxen and 0.8 mol% aescin. Black and red lines are linear fits to determine D_T .

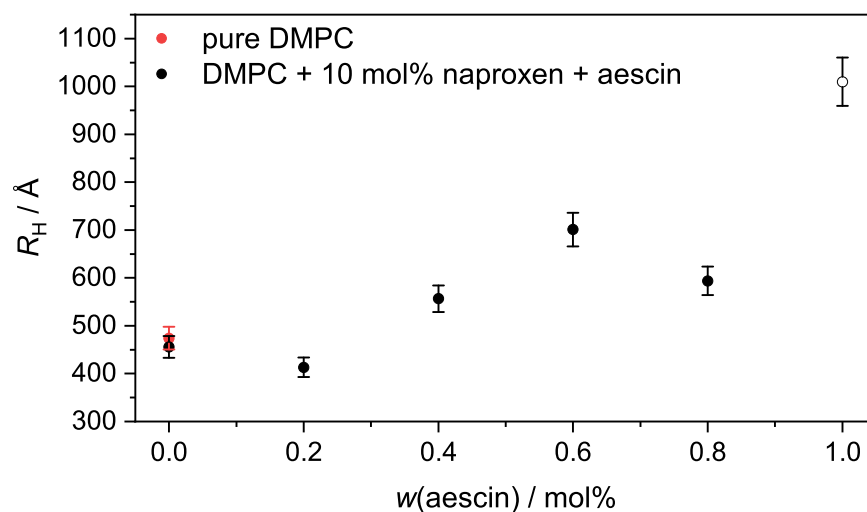


Figure 11. R_H at $T = 10^\circ \text{C}$ of the DMPC vesicles containing 10 mol% naproxen and aescin is plotted as a function of $w(\text{aescin})$. The red circle depicts the hydrodynamic radius of pure DMPC vesicles.

4. Conclusions

In this work, we analyzed DMPC model membranes containing 10 mol% of the NSAID naproxen and different amounts of the natural biosurfactant aescin (0.0 mol% to 1.0 mol%) with DSC, WAXS, SAXS, and PCS in a temperature-dependent manner. The obtained results confirm the interactions of both naproxen and aescin with the lipid bilayer formed by DMPC, independent of the method used. The obtained results were schematically summarized (see Figure 12), showing a possible scenario of the arrangement of the two additives in the lipid membrane. The intercalation of naproxen and aescin into the membrane was a priori assumed according to the publications by Alsop et al., and Sreij et al., and was evidenced with the experimental results of DSC and WAXS in this study [22,23]. The incorporation of naproxen into the DMPC membrane resulted in a lowered T_m . The addition of aescin led to a further decrease in T_m , and the formation of aescin-rich domains became visible from DSC. d_{WAXS} of the DMPC molecules increased with rising temperature, with the most significant change happening when passing T_m . At $T < T_m$, the addition of neither naproxen nor aescin showed a significant influence on d_{WAXS} . Above T_m , naproxen addition induced a decrease of d_{WAXS} and with increasing $w(\text{aescin})$, d_{WAXS} was even further reduced.

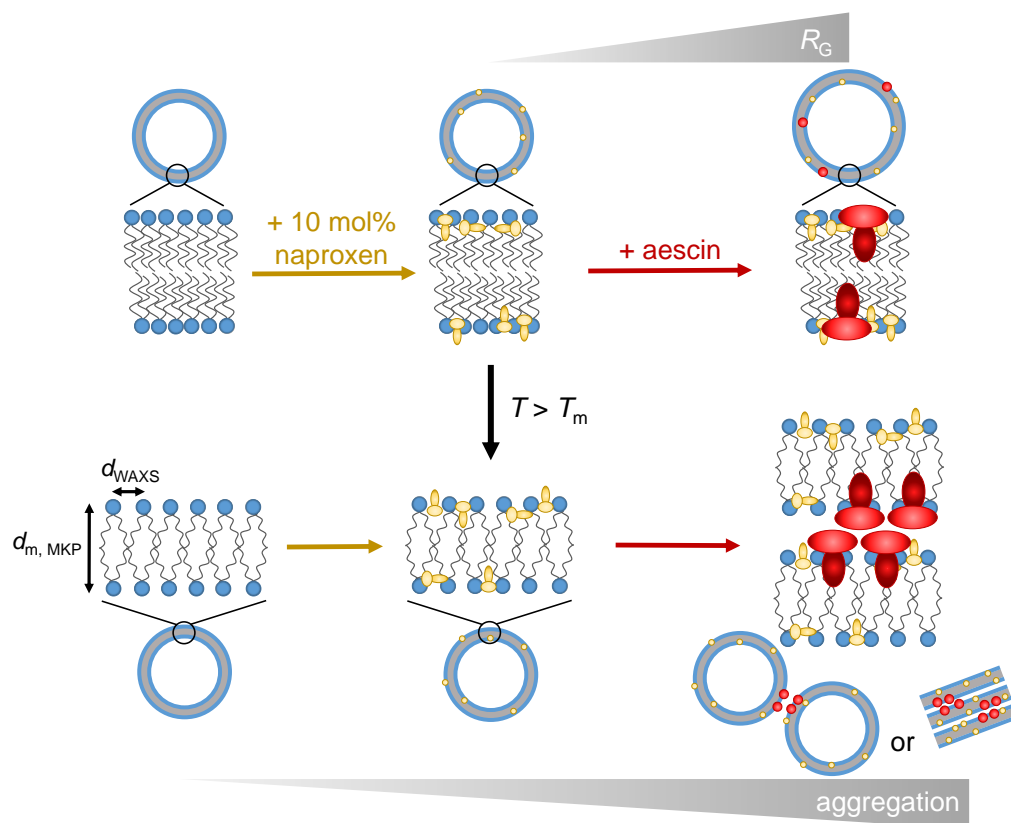


Figure 12. Schematic illustration of the proposed interplay of the drug naproxen and the saponin aescin with DMPC vesicles as model membranes. The figure displays the intercalation of both substances into the membranes and the aescin-induced formation of aggregates.

At all temperatures below T_m , well-defined small unilamellar vesicles were present, which was proven via SAXS. The membrane thickness was 34.7 Å through the MKP method at $T = 10$ °C and did not change significantly after the addition of either naproxen or aescin addition. Moreover, the addition of naproxen had no influence on R_G ; the addition of aescin, however, resulted in an increase in R_G . The vesicles tended to aggregate at $T > T_m$, which was revealed by the lamellar correlation peak. The lamellar repeat distance was constant for all aescin amounts, but the number of correlated bilayers seemed to grow by increasing $w(\text{aescin})$. This indicates that aescin acts as a linker between the two different

bilayers. Moreover, the vesicles at $T = 10\text{ }^{\circ}\text{C}$ showed a low polydispersity measured by PCS. R_H was increased by the addition of aescin.

With these measurements, both the NSAID naproxen and the saponin aescin were incorporated into the DMPC model membrane. Due to the interactions between naproxen and aescin molecules with the DMPC molecules, the membrane properties were changed. Despite the discussed differences of ibuprofen and naproxen, their effects on the DMPC model membranes were comparable. The employed methods did not resolve the type and strength of these interactions, but showed their effects on the vesicle properties. The molecular structures (see Figure 1) suggest the presence of predominantly electrostatic and hydrophobic forces [24]. A detailed analysis of the type and strength of the present forces is beyond the scope of this paper, but could be studied by methods such as avoided level crossing muon spin resonance (ALC- μ SR) to gain an insight on the orientation of additives due to the orienting effect of the electric field of the membrane [65–67]. In addition, theoretical simulations such as those by Selyutina et al. with DPFC and glycyrrhizin would be interesting to understand the DMPC-aescin-naproxen system on a more detailed level [68]. It would be very interesting to address the question of whether aescin enhances or decreases the activity of naproxen. Another scattering technique that can be used to obtain more information about the lipid bilayer and the lamellar structures is small-angle neutron scattering (SANS) [69]. Moreover, it would be a benefit to investigate these vesicles via neutron spin echo spectroscopy to obtain deeper knowledge about the fluidity and stiffness of the membrane at different phase states in the presence of naproxen and aescin [30,70]. With these results, the effect of NSAIDs and saponins on biomembranes can be better estimated for pharmaceutical applications. This understanding is of interest to expand the knowledge of interactions between biological substances and membranes. In the future, it is necessary to correlate the results obtained in this study with pharmacological studies.

Supplementary Materials: The following supporting information can be downloaded at: <https://www.mdpi.com/article/10.3390/pharmaceutics15020379/s1>, Figure S1. Temperature-dependent WAXS-curves for (a) pure DMPC, (b) DMPC with 10 mol% naproxen and (c–f) different amounts of aescin, ranging from 0.2 mol% to 0.8 mol%. The open circles mark artifacts that are not considered for evaluation. Figure S2. Temperature-dependent WAXS-curves for DMPC vesicles with 10 mol% naproxen and 1.0 mol% aescin. The open circles mark artifacts that are not considered for evaluation. Figure S3. Temperature-dependent SAXS-curves for (a) pure DMPC, (b) DMPC with 10 mol% naproxen and (c–f) different amounts of aescin, ranging from 0.2 mol% to 1.0 mol%. Curves are scaled by multiples of 10. Solid lines are IFT approximations. Figure S4. SAXS-curves of DMPC vesicles with 10 mol% naproxen and varying amounts of aescin at $T = 20\text{ }^{\circ}\text{C}$. Scattering curves are scaled by powers of 10 for better visibility. Figure S5. Γ plotted against q^2 measured by angle-dependent PCS at $T = 10\text{ }^{\circ}\text{C}$ for (a) pure DMPC, (b) DMPC with 10 mol% naproxen and (c–f) different amounts of aescin, ranging from 0.2 mol% to 0.8 mol%. Red lines are linear fits to determine D_T . Figure S6. Γ plotted against q^2 measured by angle-dependent PCS at $T = 10\text{ }^{\circ}\text{C}$ for DMPC with 10 mol% naproxen and 1.0 mol% aescin. Red lines are linear fits to determine D_T . Table S1. Hydrodynamic radius R_H and polydispersity index PDI obtained from CONTIN evaluation of PCS data in dependence on the aescin amount $w(\text{aescin})$. Data was recorded at $T = 10\text{ }^{\circ}\text{C}$. Figure S7. Comparison of R_G and R_H values, both measured at $T = 10\text{ }^{\circ}\text{C}$ and in dependence on $w(\text{aescin})$. The red symbols mark the values for pure DMPC vesicles.

Author Contributions: Conceptualization, P.H. and T.H.; investigation, P.H., F.G.-B., T.J.S. and T.B.; data evaluation, P.H. and T.B.; software (PCS), M.A.; writing—original draft preparation, P.H.; writing—review and editing, P.H., F.G.-B., M.A., C.D., T.J.S., T.B. and T.H.; visualization, P.H.; supervision, T.H. All authors have read and agreed to the published version of the manuscript.

Funding: this research received no external funding.

Institutional Review Board Statement: not applicable.

Informed Consent Statement: not applicable.

Data Availability Statement: the data are available on request from the corresponding author.

Acknowledgments: We acknowledge SOLEIL for the provision of synchrotron radiation and for access to beamline SWING (proposal 20200983). We acknowledge the support for the publication costs by the Open Access Publication Fund of Bielefeld University. We are grateful to Thomas Koop for providing the differential scanning calorimeter, and Anja Diekmann and Jan-Hendrik Peters for the support during the DSC experiments.

Conflicts of Interest: the authors declare no conflict of interest.

References

1. Singer, S.J.; Nicolson, G.L. The Fluid Mosaic Model of the Structure of Cell Membranes. *Science* **1972**, *175*, 720–731. [[CrossRef](#)] [[PubMed](#)]
2. Eddidin, M. Lipids on the frontier: A century of cell-membrane bilayers. *Nat. Rev. Mol. Cell Biol.* **2003**, *4*, 414–418. [[CrossRef](#)]
3. Kiselev, M.A. Methods for Lipid Nanostructure Investigation at Neutron and Synchrotron Sources. *Phys. Part. Nucl.* **2011**, *42*, 302–331. [[CrossRef](#)]
4. Cevc, G. Lipid vesicles and other colloids as drug carriers on the skin. *Adv. Drug Deliv. Rev.* **2004**, *56*, 675–711. [[CrossRef](#)] [[PubMed](#)]
5. Li, J.; Wang, X.; Zhang, T.; Wang, C.; Huang, Z.; Luo, X.; Deng, Y. A review on phospholipids and their main applications in drug delivery systems. *Asian J. Pharm. Sci.* **2015**, *10*, 81–98. [[CrossRef](#)]
6. Hope, M.J.; Bally, M.B.; Mayer, L.D.; Janoff, A.S.; Cullis, P.R. Generation of multilamellar and unilamellar phospholipid vesicles. *Chem. Phys. Lipids* **1986**, *40*, 89–107. [[CrossRef](#)]
7. MacDonald, R.C.; MacDonald, R.I.; Menco, B.P.; Takeshita, K.; Subbarao, N.K.; Hu, L.R. Small-volume extrusion apparatus for preparation of large, unilamellar vesicles. *Biochim. Biophys. Acta (BBA)—Biomembr.* **1991**, *1061*, 297–303. [[CrossRef](#)]
8. Akbarzadeh, A.; Rezaei-Sadabady, R.; Davaran, S.; Joo, S.W.; Zarghami, N.; Hanifehpour, Y.; Samiei, M.; Kouhi, M.; Nejati-Koshki, K. Liposome: Classification, preparation, and applications. *Nanoscale Res. Lett.* **2013**, *8*, 102. [[CrossRef](#)]
9. Ulrich, A.S. Biophysical Aspects of Using Liposomes as Delivery Vehicles. *Biosci. Rep.* **2002**, *22*, 129–150. [[CrossRef](#)]
10. Du, L.; Liu, X.; Huang, W.; Wang, E. A study on the interaction between ibuprofen and bilayer lipid membrane. *Electrochim. Acta* **2006**, *51*, 5754–5760. [[CrossRef](#)]
11. Samad, A.; Sultana, Y.; Aqil, M. Liposomal Drug Delivery Systems: An Update Review. *Curr. Drug Deliv.* **2007**, *4*, 297–305. [[CrossRef](#)]
12. de Meyer, F.J.M.; Benjamini, A.; Rodgers, J.M.; Misteli, Y.; Smit, B. Molecular Simulation of the DMPC-Cholesterol Phase Diagram. *J. Phys. Chem. B* **2010**, *114*, 10451–10461. [[CrossRef](#)]
13. Koynova, R.; Caffrey, M. Phases and phase transitions of the phosphatidylcholines. *Biochim. Biophys. Acta (BBA)—Rev. Biomembr.* **1998**, *1376*, 91–145. [[CrossRef](#)]
14. Todd, P.A.; Clissold, S.P. Naproxen. A Reappraisal of its Pharmacology, and Therapeutic Use in Rheumatic Diseases and Pain States. *Drugs* **1990**, *40*, 91–137. [[CrossRef](#)]
15. Manrique-Moreno, M.; Garidel, P.; Suwalsky, M.; Howe, J.; Brandenburg, K. The membrane-activity of Ibuprofen, Diclofenac, and Naproxen: A physico-chemical study with lecithin phospholipids. *Biochim. Biophys. Acta* **2009**, *1788*, 1296–1303. [[CrossRef](#)] [[PubMed](#)]
16. Yousefpour, A.; Amjad Iranagh, S.; Nademi, Y.; Modarress, H. Molecular dynamics simulation of nonsteroidal antiinflammatory drugs, naproxen and relafen, in a lipid bilayer membrane. *Int. J. Quantum Chem.* **2013**, *113*, 1919–1930. [[CrossRef](#)]
17. Brooks, P. Use and Benefits of Nonsteroidal Anti-inflammatory Drugs. *Am. J. Med.* **1998**, *104*, 9S–13S. [[CrossRef](#)]
18. Boggara, M.B.; Krishnamoorti, R. Small-Angle Neutron Scattering Studies of Phospholipid-NSAID Adducts. *Langmuir ACS J. Surfaces Colloids* **2010**, *26*, 5734–5745. [[CrossRef](#)] [[PubMed](#)]
19. Pereira-Leite, C.; Figueiredo, M.; Burdach, K.; Nunes, C.; Reis, S. Unraveling the Role of Drug-Lipid Interactions in NSAIDs-Induced Cardiotoxicity. *Membranes* **2020**, *11*, 24. [[CrossRef](#)]
20. Sharma, V.K.; Mamontov, E.; Tyagi, M. Effects of NSAIDs on the Nanoscopic Dynamics of Lipid Membrane. *Biochim. Biophys. Acta. Biomembr.* **2020**, *1862*, 183100. [[CrossRef](#)]
21. Przykaza, K.; Jurak, M.; Wiącek, A.E. Effect of naproxen on the model lipid membrane formed on the water-chitosan subphase. *Biochim. Biophys. Acta. Biomembr.* **2022**, *1865*, 184099. [[CrossRef](#)] [[PubMed](#)]
22. Sreij, R.; Prévost, S.; Dargel, C.; Dattani, R.; Hertle, Y.; Wrede, O.; Hellweg, T. Interaction of the Saponin Aescin with Ibuprofen in DMPC Model Membranes. *Mol. Pharm.* **2018**, *15*, 4446–4461. [[CrossRef](#)] [[PubMed](#)]
23. Alsop, R.J.; Armstrong, C.L.; Maqbool, A.; Topozini, L.; Dies, H.; Rheinstädter, M.C. Cholesterol expels ibuprofen from the hydrophobic membrane core and stabilizes lamellar phases in lipid membranes containing ibuprofen. *Soft Matter* **2015**, *11*, 4756–4767. [[CrossRef](#)] [[PubMed](#)]
24. Lichtenberger, L.M.; Wang, Z.M.; Romero, J.J.; Ulloa, C.; Perez, J.C.; Giraud, M.N.; Barreto, J.C. Non-steroidal anti-inflammatory drugs (NSAIDs) associate with zwitterionic phospholipids: Insight into the mechanism and reversal of NSAID-induced gastrointestinal injury. *Nat. Med.* **1995**, *1*, 154–158. [[CrossRef](#)]
25. Cheok, C.Y.; Salman, H.A.K.; Sulaiman, R. Extraction and quantification of saponins: A review. *Food Res. Int.* **2014**, *59*, 16–40. [[CrossRef](#)]

26. Böttcher, S.; Drusch, S. Saponins - Self-assembly and behavior at aqueous interfaces. *Adv. Colloid Interface Sci.* **2017**, *243*, 105–113. [[CrossRef](#)]
27. Böttger, S.; Hofmann, K.; Melzig, M.F. Saponins can perturb biologic membranes and reduce the surface tension of aqueous solutions: A correlation? *Bioorg. Med. Chem.* **2012**, *20*, 2822–2828. [[CrossRef](#)]
28. Güçlü-Ustündağ, O.; Mazza, G. Saponins: Properties, Applications and Processing. *Crit. Rev. Food Sci. Nutr.* **2007**, *47*, 231–258. [[CrossRef](#)]
29. Sparg, S.G.; Light, M.E.; van Staden, J. Biological activities and distribution of plant saponins. *J. Ethnopharmacol.* **2004**, *94*, 219–243. [[CrossRef](#)]
30. Sreij, R.; Dargel, C.; Geisler, P.; Hertle, Y.; Radulescu, A.; Pasini, S.; Perez, J.; Moleiro, L.H.; Hellweg, T. DMPC vesicle structure and dynamics in the presence of low amounts of the saponin aescin. *Phys. Chem. Chem. Phys. PCCP* **2018**, *20*, 9070–9083. [[CrossRef](#)]
31. Sreij, R.; Dargel, C.; Hannappel, Y.; Jestin, J.; Prévost, S.; Dattani, R.; Wrede, O.; Hellweg, T. Temperature dependent self-organization of DMPC membranes promoted by intermediate amounts of the saponin aescin. *Biochim. Biophys. Acta. Biomembr.* **2019**, *1861*, 897–906. [[CrossRef](#)]
32. Dargel, C.; Hannappel, Y.; Hellweg, T. Heating-Induced DMPC/Glycyrrhizin Bicelle-to-Vesicle Transition: A X-Ray Contrast Variation Study. *Biophys. J.* **2020**, *118*, 2411–2425. [[CrossRef](#)]
33. Geisler, R.; Prévost, S.; Dattani, R.; Hellweg, T. Effect of Cholesterol and Ibuprofen on DMPC- β -Aescin Bicelles: A Temperature-Dependent Wide-Angle X-ray Scattering Study. *Crystals* **2020**, *10*, 401. [[CrossRef](#)]
34. Geisler, R.; Pedersen, M.C.; Preisig, N.; Hannappel, Y.; Prévost, S.; Dattani, R.; Arleth, L.; Hellweg, T. Aescin - a natural soap for the formation of lipid nanodiscs with tunable size. *Soft Matter* **2021**, *17*, 1888–1900. [[CrossRef](#)] [[PubMed](#)]
35. Lorent, J.H.; Quetin-Leclercq, J.; Mingeot-Leclercq, M.P. The amphiphilic nature of saponins and their effects on artificial and biological membranes and potential consequences for red blood and cancer cells. *Org. Biomol. Chem.* **2014**, *12*, 8803–8822. [[CrossRef](#)] [[PubMed](#)]
36. Matsuda, H.; Li, Y.; Murakami, T.; Ninomiya, K.; Yamahara, J.; Yoshikawa, M. Effects of Escins Ia, Ib, IIa, and IIb from Horse Chestnut, the Seeds of *Aesculus hippocastanum* L., on Acute Inflammation in Animals. *Biol. Pharm. Bull.* **1997**, *20*, 1092–1095. [[CrossRef](#)] [[PubMed](#)]
37. Pekdemir, T.; Ishigami, Y.; Uchiyama, H. Characterization of Aescin as a Biosurfactant for Environmental Remediation. *J. Surfactants Deterg.* **1999**, *2*, 337–341. [[CrossRef](#)]
38. Sirtori, C.R. Aescin: Pharmacology, pharmacokinetics and therapeutic profile. *Pharmacol. Res.* **2001**, *44*, 183–193. [[CrossRef](#)]
39. Dargel, C.; Geisler, R.; Hannappel, Y.; Kemker, I.; Sewald, N.; Hellweg, T. Self-Assembly of the Bio-Surfactant Aescin in Solution: A Small-Angle X-ray Scattering and Fluorescence Study. *Colloids Interfaces* **2019**, *3*, 47. [[CrossRef](#)]
40. Wilkinson, J.A.; Brown, A.M. Horse chestnut - *Aesculus Hippocastanum*: Potential applications in cosmetic skin-care products. *Int. J. Cosmet. Sci.* **1999**, *21*, 437–447. [[CrossRef](#)] [[PubMed](#)]
41. Patlolla, J.M.R.; Rao, C.V. Anti-inflammatory and Anti-cancer Properties of β -Escin, a Triterpene Saponin. *Curr. Pharmacol. Rep.* **2015**, *1*, 170–178. [[CrossRef](#)]
42. Pittler, M.H.; Ernst, E. Horse-Chestnut Seed Extract for Chronic Venous Insufficiency. A Criteria-Based Systematic Review. *Arch. Dermatol.* **1998**, *134*, 1356–1360. [[CrossRef](#)]
43. Geisler, R.; Dargel, C.; Hellweg, T. The Biosurfactant β -Aescin: A Review on the Physico-Chemical Properties and Its Interaction with Lipid Model Membranes and Langmuir Monolayers. *Molecules* **2019**, *25*, 117. [[CrossRef](#)]
44. Sreij, R.; Dargel, C.; Moleiro, L.H.; Monroy, F.; Hellweg, T. Aescin Incorporation and Nanodomain Formation in DMPC Model Membranes. *Langmuir ACS J. Surfaces Colloids* **2017**, *33*, 12351–12361. [[CrossRef](#)]
45. Geisler, R.; Pedersen, M.C.; Hannappel, Y.; Schweins, R.; Prévost, S.; Dattani, R.; Arleth, L.; Hellweg, T. Aescin-Induced Conversion of Gel-Phase Lipid Membranes into Bicelle-like Lipid Nanoparticles. *Langmuir ACS J. Surfaces Colloids* **2019**, *35*, 16244–16255. [[CrossRef](#)]
46. Bushra, R.; Aslam, N. An overview of clinical pharmacology of Ibuprofen. *Oman Med. J.* **2010**, *25*, 155–1661. [[CrossRef](#)]
47. Vree, T.B.; van den Biggelaar-Martea, M.; Verwey-van Wissen, C.P.; Vree, J.B.; Guelen, P.J. Pharmacokinetics of naproxen, its metabolite O-desmethylnaproxen, and their acyl glucuronides in humans. *Biopharm. Drug Dispos.* **1993**, *14*, 491–502. [[CrossRef](#)]
48. Albozahid, M.; Naji, H.Z.; Alobad, Z.K.; Wychowanec, J.K.; Saiani, A. Synthesis and characterization of hard copolymer polyurethane/functionalized graphene nanocomposites: Investigation of morphology, thermal stability, and rheological properties. *J. Appl. Polym. Sci.* **2022**, *139*, e53118. [[CrossRef](#)]
49. Bunjes, H.; Unruh, T. Characterization of lipid nanoparticles by differential scanning calorimetry, X-ray and neutron scattering. *Adv. Drug Deliv. Rev.* **2007**, *59*, 379–402. [[CrossRef](#)]
50. Narayanan, T.; Kononov, O. Synchrotron Scattering Methods for Nanomaterials and Soft Matter Research. *Materials* **2020**, *13*, 752. [[CrossRef](#)] [[PubMed](#)]
51. Viguier, G.; Girardot, R.; Perez, J. Foxtrot, 2016. Available online: www.synchrotron-soleil.fr/en/beamlines/swing (accessed on 14 January 2023).
52. Marsh, D. Lateral order in gel, subgel and crystalline phases of lipid membranes: Wide-angle X-ray scattering. *Chem. Phys. Lipids* **2012**, *165*, 59–76 [[CrossRef](#)] [[PubMed](#)]
53. Sztucki, M. SAXSutilities2: A graphical user interface for processing and analysis of Small-Angle X-ray Scattering data. *Zenodo*, 21 September 2021. [[CrossRef](#)]

54. Glatter, O. A New Method for the Evaluation of Small-Angle Scattering Data. *J. Appl. Crystallogr.* **1977**, *10*, 415–421. [[CrossRef](#)]
55. Bergmann, A.; Fritz, G.; Glatter, O. Solving the generalized indirect Fourier transformation (GIFT) by Boltzmann simplex simulated annealing (BSSA). *J. Appl. Crystallogr.* **2000**, *33*, 1212–1216. [[CrossRef](#)]
56. Kucerka, N.; Kiselev, M.A.; Balgavý, P. Determination of bilayer thickness and lipid surface area in unilamellar dimyristoylphosphatidylcholine vesicles from small-angle neutron scattering curves: A comparison of evaluation methods. *Eur. Biophys. J. EBJ* **2004**, *33*, 328–334. [[CrossRef](#)]
57. Provencher, S.W. CONTIN: A general purpose constrained regularization program for inverting noisy linear algebraic and integral equations. *Comput. Phys. Commun.* **1982**, *27*, 229–242. [[CrossRef](#)]
58. Provencher, S.W. A constrained regularization method for inverting data represented by linear algebraic or integral equations. *Comput. Phys. Commun.* **1982**, *27*, 213–227. [[CrossRef](#)]
59. Stetefeld, J.; McKenna, S.A.; Patel, T.R. Dynamic light scattering: A practical guide and applications in biomedical sciences. *Biophys. Rev.* **2016**, *8*, 409–427. [[CrossRef](#)]
60. Cho, C.H.; Urquidi, J.; Singh, S.; Robinson, G.W. Thermal Offset Viscosities of Liquid H₂O, D₂O, and T₂O. *J. Phys. Chem. B* **1999**, *103*, 1991–1994. [[CrossRef](#)]
61. Manrique-Moreno, M.; Villena, F.; Sotomayor, C.P.; Edwards, A.M.; Muñoz, M.A.; Garidel, P.; Suwalsky, M. Human cells and cell membrane molecular models are affected in vitro by the nonsteroidal anti-inflammatory drug ibuprofen. *Biochim. Biophys. Acta* **2011**, *1808*, 2656–2664. [[CrossRef](#)]
62. Caracciolo, G.; Pozzi, D.; Caminiti, R.; Marchini, C.; Montani, M.; Amici, A.; Amenitsch, H. Transfection efficiency boost by designer multicomponent lipoplexes. *Biochim. Biophys. Acta* **2007**, *1768*, 2280–2292. [[CrossRef](#)]
63. Tristram-Nagle, S. Use of X-Ray and Neutron Scattering Methods with Volume Measurements to Determine Lipid Bilayer Structure and Number of Water Molecules/Lipid. *Sub-Cell. Biochem.* **2015**, *71*, 17–43. [[CrossRef](#)]
64. Kiselev, M.A.; Lombardo, D. Structural characterization in mixed lipid membrane systems by neutron and X-ray scattering. *Biochim. Biophys. Acta. Gen. Subj.* **2017**, *1861*, 3700–3717. [[CrossRef](#)] [[PubMed](#)]
65. McKenzie, I.; Scheuermann, R.; Tucker, I.; Mulley, B.P. Dynamics and local environment of an aromatic counterion bound to di-chain cationic surfactant bilayers studied by avoided level crossing muon spin resonance: Evidence for counterion condensation. *Phys. Chem. Chem. Phys.* **2021**, *23*, 25542–25549. [[CrossRef](#)]
66. Martyniak, A.; Scheuermann, R.; Dilger, H.; Tucker, I.M.; Burkert, T.; Hashmi, A.; Vujošević, D.; Roduner, E. Solvation thermodynamics of phenylalcohols in lamellar phase surfactant dispersions. *Phys. B Condens. Matter* **2006**, *374–375*, 328–331. [[CrossRef](#)]
67. Roduner, E. Muons, soap, and drug delivery—An invitation to enter a new field of research. *Phys. B Condens. Matter* **2003**, *326*, 19–24. [[CrossRef](#)]
68. Selyutina, O.Y.; Apanasenko, I.E.; Kim, A.V.; Shelepova, E.A.; Khalikov, S.S.; Polyakov, N.E. Spectroscopic and molecular dynamics characterization of glycyrrhizin membrane-modifying activity. *Colloids Surfaces. B Biointerfaces* **2016**, *147*, 459–466 [[CrossRef](#)]
69. Bergström, M.; Pedersen, J.S.; Schurtenberger, P.; Egelhaaf, S.U. Small-Angle Neutron Scattering (SANS) Study of Vesicles and Lamellar Sheets Formed from Mixtures of an Anionic and a Cationic Surfactant. *J. Phys. Chem. B* **1999**, *103*, 9888–9897. [[CrossRef](#)]
70. Boggara, M.B.; Faraone, A.; Krishnamoorti, R. Effect of pH and ibuprofen on the phospholipid bilayer bending modulus. *J. Phys. Chemistry. B* **2010**, *114*, 8061–8066. [[CrossRef](#)]

Disclaimer/Publisher’s Note: The statements, opinions and data contained in all publications are solely those of the individual author(s) and contributor(s) and not of MDPI and/or the editor(s). MDPI and/or the editor(s) disclaim responsibility for any injury to people or property resulting from any ideas, methods, instructions or products referred to in the content.